ADVANCED FUNCTIONAL MATERIALS
www.afm-journal.de

Red AIE-Active Fluorescent Probes with Tunable Organelle-Specific Targeting

*Parvej Alam, Wei He, Nelson L. C. Leung, Chao Ma, Ryan T. K. Kwok, Jacky W. Y. Lam, Herman H. Y. Sung, Ian D. Williams, Kam Sing Wong, and Ben Zhong Tang**

Cell staining is a fascinating research area where monitoring and visualizing different cell organelles can be done using fluorescence techniques. However, the design and synthesis of organelle-targeting fluorophores is still a challenge for several specific organelles. Herein, a platform for synthesizing efficient red-emitting aggregation-induced emission luminogens (AIEgens) with donor–acceptor characteristics is reported. The core molecule can be easily functionalized in order to modulate organelle targeting. The three synthesized AIEgens exhibit quantum yields of up to 39.3% and two-photon absorption cross-section values of up to 162 GM. The two zwitterionic AIEgens, CDPP-3SO_3 and CDPP-4SO_3, with the sulfonate function group, are successfully utilized for specific one-photon and two-photon imaging of the endoplasmic reticulum (ER) in live human cells. Substituting the zwitterionic nature with a singly positive charge group, one-photon and two-photon imaging of CDPP-BzBr shows mitochondrial specificity, indicating the importance of the zwitterionic group for ER-targeting. Owing to the good in vitro photostability, cell viability, and high efficiency, these red dyes serve as a good potential candidate for specific organelle targeting, as well as illustrate how such a platform can easily aid in the study of structure–property relationships for designing such probes.

1. Introduction

Cells are fundamental building blocks for living organisms.[1,2] Indeed, the human body is made of trillions of cells each with their own specific functionality.[3] Each cell is made up of cellular organelles, such as the plasma membrane, mitochondria, lysosomes, Golgi apparatus, and endoplasmic reticulum (ER).[4] Though it has long been known that these structures are vital for cellular operation and consequently, the whole body, further study has revealed more detailed understanding of their significance pertaining to specific biochemical processes and pathways.[5–7] Due to their nature and size, the study of organelles, their health, and their function can be technically difficult. For a long time, there was limited tools to study such important structures.[8] With the development of fluorescent bioprobes, researchers became able to visualize the once invisible organelles revealing important and significant insight.[9,10] Development of the bioprobes has resulted in organelle specific staining agents allowing researchers to study the targeted organelle.[11–15] The visualization techniques reveal the location and morphology of the organelles, and thus enable the study and monitoring of changes that reveal important biological states or dysfunction.[16] In particular, super-resolution microscopy is able to provide unprecedented clarity into the morphology of these structures.[17–19]

Fluorescent probes have greatly aided the study of cellular structures and biochemical processes, but due to the hydrophobic π-conjugated backbone of conventional dyes, many of these systems suffer aggregation-caused quenching (ACQ), a reduction in emission efficiency when the molecules interact with each other.[20,21] The ACQ phenomenon can be particularly egregious when the conventional dyes are used for bioimaging applications due to the highly polar nature of the aqueous media in cells, easily leading the dye molecules to aggregate together in even slightly higher concentrations. Thus, typical cell staining dyes are used in nanomolar concentrations to circumvent such issues. However, at such concentrations, quenching due to photobleaching becomes much more pronounced. Though researchers have come up with a variety of ingenious methods to overcome the issue of ACQ, there has been much work successfully incorporating molecules

Dr. P. Alam, W. He, Dr. N. L. C. Leung, Dr. R. T. K. Kwok, Dr. J. W. Y. Lam, Dr. H. H. Y. Sung, Prof. I. D. Williams, Prof. B. Z. Tang
Department of Chemistry
Hong Kong Branch of Chinese National Engineering Research Center for Tissue Restoration and Reconstruction
Department of Chemical and Biological Engineering
The Hong Kong University of Science and Technology
Clear Water Bay, Kowloon, Hong Kong 999077, China
E-mail: tangbenz@ust.hk

C. Ma, Prof. K. S. Wong
Department of Physics
The Hong Kong University of Science and Technology
Clear Water Bay, Kowloon, Hong Kong 999077, China

Prof. B. Z. Tang
Center for Aggregation-Induced Emission
SCUT-HKUST Joint Research Institute
State Key Laboratory of Luminescent Materials and Devices
South China University of Technology
Guangzhou 510640, China

W. He, Dr. R. T. K. Kwok, Prof. B. Z. Tang
HKUST-Shenzhen Research Institute
No. 9 Yuexing 1st RD, South Area, Hi-tech Park, Nanshan, Shenzhen 518057, China

The ORCID identification number(s) for the author(s) of this article can be found under https://doi.org/10.1002/adfm.201909268.

DOI: 10.1002/adfm.201909268

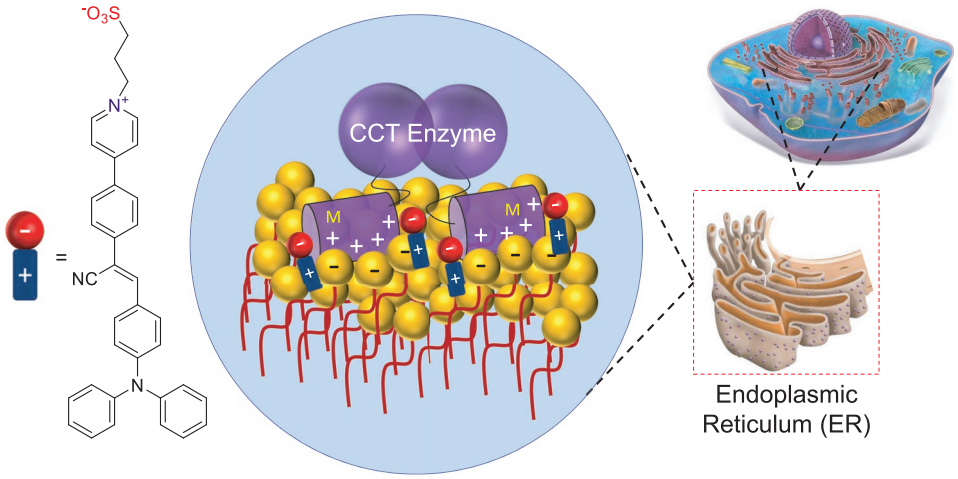

Figure 1. Schematic representation of specific endoplasmic reticulum (ER) targeting by zwitterionic AIEgens. Choline phosphate cytidylyltransferase (CCT), a membrane-bound enzyme, is found on the ER and is a key enzyme involved in phosphatidylcholine synthesis.

exhibiting aggregation-induced emission (AIE) for a multitude of applications, including cell staining, in vivo imaging, and theranostics.[22–29] The concept of AIE describes a phenomenon whereby emission is observed when the luminogen aggregates with other molecules. Typically, this luminogen is originally nonemissive or weakly emissive due to molecular motions which allow the molecule to decay nonradiatively. Upon aggregation or binding to molecules, such molecular motions become restricted, forcing the molecule to decay via radiative pathways, turning on emission.[30]

From our previous structure–property relationship research regarding AIE systems for cell imaging studies, we have observed a number of molecular designs that allow for specific organelle targeting and staining: small hydrophobic systems are drawn to lipid droplets; hydrophobic molecules with long alkyl chains target the phospholipid bilayer; positively charged compounds stain the mitochondria due to the organelle's membrane potential.[11,31–33] However, there have been limited examples of molecules that are capable of staining the ER.[34–40] The ER is a large membrane-bound compartment spread throughout the cytoplasm of eukaryotic cells, which is composed of one completely continuous membrane bilayer and has a single continuous lumen. The ER plays a key role in cellular metabolism, protein synthesis, and the transport of intermediates and signaling molecules.[34,41–43] Characterization of the ER structure in living cells is challenging due to a wide 3D interconnected network of flattened, membrane-enclosed sacks or tube-like cisterns and tubules with different thicknesses.[44,45]

Herein we designed a simple platform using an AIE-active molecule that facilitates the rational design and synthesis of bioprobes. One main feature of the core molecule is its donor–π–pyridine design, since the pyridine molecule allows researchers to easily control functionalization and thus, functionality. Upon functionalization, the pyridine becomes a pyridinium strengthening the donor–acceptor properties of the molecule bathochromically shifting emission to deep-red wavelengths, ideal for bioimaging applications, with acceptable to great quantum yields. The ease of modification also simplifies studies regarding structure–property relationships. In our case, we were able to observe that the zwitterionic nature of the pyridinium-sulfonate group seems to allow ER targeting, with the singly positive charged molecule only targeting the mitochondria. The selectivity towards the ER could be due to an abundance of the phosphocholine cytidylyltransferase (CCT), a key enzyme in regulating membrane phospholipid synthesis, on the ER membrane.[46–48] As the α-helix (domain M) of CCT contains multiple positively charged amino acids and selectively binds to anionic membrane surfaces, we hypothesized that the zwitterionic probes might bind to such locations due to their oppositely matching charges via electrostatic interactions (**Figure 1**).[49,50]

2. Results and Discussion

2.1. Molecular Design, Synthesis, and Characterization

The synthesis of fluorescent probes with long emission wavelength >550 nm can be achived by connecting electron-accepting (A) units with electron-donating (D) units via π-bridge(s), i.e., D–π–A organic systems. In our strategy, an electron-donating group, the propeller shaped triphenylamine (TPA) segment, was chosen as a D unit; an AIE active core, the α-cyanostilbene, as a π-bridge; and an electron-accepting unit, the pyridinium, as the A unit. The core molecule (*Z*)-4-(4-(1-cyano-2-(4-(diphenylamino)phenyl)vinyl)phenyl)pyridin-1-ium (CDPP) was synthesized by a two-step reaction: i) a Knoevenagel condensation between 4-(diphenylamino)benzaldehyde and 2-(4-bromophenyl)acetonitrile, followed by ii) a Suzuki coupling with 4-pyridine boronic acid, yielding yellow powder with a total yield of 73% (Scheme S1, Supporting Information).[51] Finally, the targeted fluorophores CDPP-3SO_3, CDPP-4SO_3, and CDPP-BzBr, were synthesized by simple reactions between CDPP and 1,3-propane sultone, 1,4-butane sultone, and 4-bromobenzyl bromide, respectively (**Figure 2**A; Scheme S1, Supporting Information).[51–53] The chemical structures of all the synthesized compounds were characterized by standard spectroscopic techniques such as ^{1}H NMR, ^{13}C NMR, and high-resolution mass spectroscopy (HRMS) (Figures S1–S5, Supporting Information).

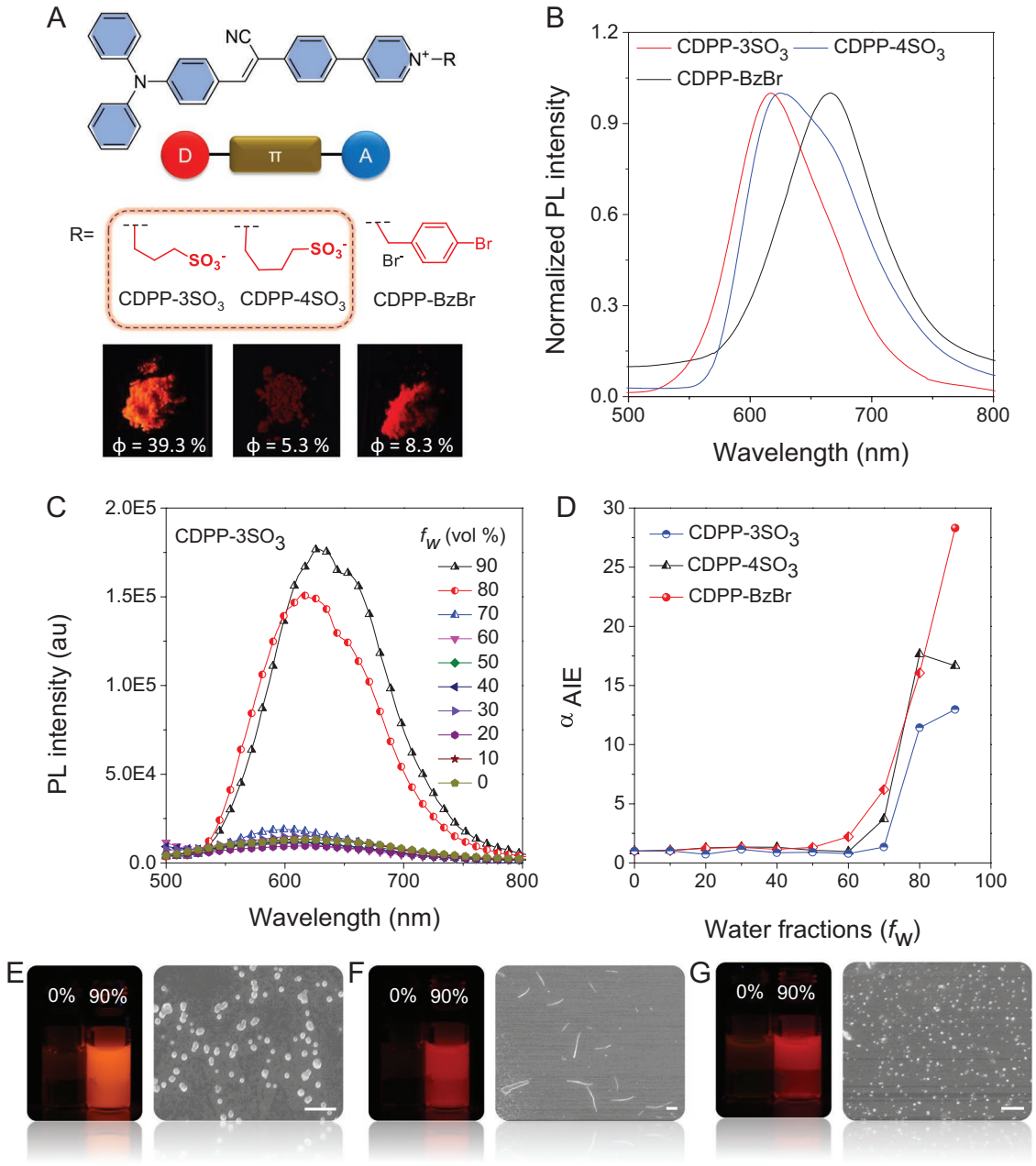

Figure 2. A) Molecular structures of CDPP derivatives and photographs of all three compounds under 365 nm UV excitation, including their solid-state quantum yield (Φ). B) Fluorescence spectra of CDPP-3SO_3, CDPP-4SO_3, and CDPP-BzBr in solid state. C) PL spectra of CDPP-3SO_3 in DMSO/water mixtures with different water fractions (f_w); concentration = 10×10^{-6} M. D) Plots of PL maximum and relative PL intensity ($\alpha_{AIE} = I/I_0$) versus the composition of the DMSO/water mixture of CDPP-3SO_3, CDPP-4SO_3, and CDPP-BzBr, where I_0 was the PL intensity at $f_w = 0\%$; concentration = 10×10^{-6} M, $\lambda_{ex} = 480$ nm. The fluorescence photograph at $f_w = 0\%$ and 90% and the corresponding SEM image of the nanoaggregates collected at $f_w = 90\%$ of E) CDPP-3SO_3, F) CDPP-4SO_3, and G) CDPP-BzBr; scale bar: 1 µm. The photographs were taken under 365 nm UV irradiation from a hand-held UV lamp. [CDPP = (*Z*)-4-(4-(1-cyano-2-(4-diphenylamino)phenyl)vinyl)phenyl)pyridin-1-ium].

2.2. Optical Properties

The compounds in general exhibited poor solubility in many polar solvents and were not visibly soluble in nonpolar solvents. Optical properties, absorption and emission spectra, of CDPP-3SO_3, CDPP-4SO_3, and CDPP-BzBr were investigated in dimethyl sulfoxide (DMSO) at room temperature. The absorption spectra of CDPP-3SO_3, CDPP-4SO_3, and CDPP-BzBr showed similar absorption maxima at ≈480 nm (Figure S6A, Supporting Information). The emission spectra of CDPP-3SO_3, CDPP-4SO_3, and CDPP-BzBr were found in the range of 585 to 620 nm in DMSO (Figure S6B, Supporting Information). The solid-state efficiency of CDPP-3SO_3, CDPP-4SO_3, and CDPP-BzBr was found to be 39.3%, 5.3%,

and 8.3%, respectively (Figure 2A). The solid-state emission of CDPP-$3SO_3$ and CDPP-$4SO_3$ showed similar emission maxima at ≈620 nm however CDPP-BzBr showed red shifted emission at 665 nm compare to CDPP-$3SO_3$ and CDPP-$4SO_3$ (Figure 2B).

It is evident that the AIE molecules are highly affected by the rigidity of their environment. Comparing CDPP-$3SO_3$ and CDPP-$4SO_3$, the butyl linker of the latter may increase disorder resulting in a less rigid environment reducing solid state quantum yield. From the crystal packing of CDPP-$3SO_3$, we see the existence of π–π stacking interactions. These interactions likely exist for CDPP-BzBr as evidenced by the red shifting of its solid-state emission. The degree of red-shifting likely indicates the strength of the π–π interaction which ultimately results in lowering the solid state QY.

Furthermore, the emission behavior of CDPP-$3SO_3$, CDPP-$4SO_3$, and CDPP-BzBr were studied in DMSO/water solvent mixtures to evaluate their aggregation properties. For CDPP-$3SO_3$, increasing the water fraction in DMSO/water mixtures from 0% to 60% resulted in no visible changes in the photoluminescence (PL) intensity. When $f_w \geq 70\%$, emission intensity became enhanced alongside a bathochromic shift (from 620 to 640 nm), signaling the formation of nanoaggregates. The maximum PL intensity was observed at $f_w = 90\%$ and α_{AIE} or I/I_0 was found to be ≈14. Similar AIE behavior was observed for CDPP-$4SO_3$ and CDPP-BzBr in the presence of different DMSO/water mixtures and their α_{AIE} was found to be ≈17 and 30, respectively (Figure 2C,D; Figures S7 and S8, Supporting Information). Additionally, scanning electron microscopy (SEM) was performed to validate aggregate formation when $f_w = 90\%$ (Figure 2E–G). SEM revealed that the CDPP-$3SO_3$ and CDPP-BzBr formed spherical shaped nanoaggregates. CDPP-$4SO_3$, however, formed wire-shaped nanoaggregates (Figure 2F). Fluorescence decay measurements of CDPP-$3SO_3$, CDPP-$4SO_3$, and CDPP-BzBr nanoaggregates at $f_w = 90\%$ revealed that their lifetimes were 2.1, 2.0, and 2.0 ns, respectively (Figure S9, Supporting Information).

2.3. Single X-Ray Crystallography

One of the synthesized compounds, CDPP-$3SO_3$ was successfully characterized by single crystal X-ray diffraction (SXRD) (**Figure 3**A). The propeller conformation of TPA showed dihedral angles of 54.1°, 68.1°, and 74.2° among the three phenyl rings. The crystal packing showed various CH$\cdots\pi$, $\pi\cdots\pi$, and CH/$\pi\cdots$O interactions, which were measured to be in the range of 2.72–2.89, 3.39–3.87, and 2.32–3.12 Å, respectively (Figure 3B,C), with a centroid-to-centroid distance of 3.87 Å (Figure 3B). It is speculated that the propeller conformation allows for molecular motions which lead to nonradiative decay pathways in the solution state. However, the short interactions suppress molecular motions inhibiting nonradiative decay and open new radiative channels in the aggregate/solid state.

2.4. Cell Imaging Studies

The specific ER targeting ability of CDPP-$3SO_3$ and CDPP-$4SO_3$ was demonstrated by co-staining HeLa cells with ER-Tracker Red, one of the frequently adopted probes for ER-staining. Both CDPP-$3SO_3$ and CDPP-$4SO_3$ can efficiently stain the cell within 1 h at 1×10^{-6} M. The fluorescent area matches very well with those of ER-Tracker Red with a high Pearson's correlation factor at 0.85 for CDPP-$3SO_3$, and 0.86 for CDPP-$4SO_3$, indicating that these AIEgens can selectively target ER (**Figure 4**; Figure S10, Supporting Information).

In addition, Mito-Tracker Deep Red was employed to investigate the subcellular localization pattern of CDPP-$3SO_3$ and CDPP-$4SO_3$, with the resultant images clearly indicating that their staining region only partially overlapped with Mito-Tracker Deep Red. The Pearson's correlation values between Mito-Tracker Deep Red and CDPP-$3SO_3$ was 0.55 and 0.57 for CDPP-$4SO_3$, suggesting that these AIEgens did not stain mitochondria in HeLa. Moreover, we were also able to successfully verify the ER staining property of CDPP-$3SO_3$ when employed to stain 143B cells (Figure S11, Supporting Information).

To investigate the importance of the zwitterionic functional group, we designed the molecule CDPP-BzBr (Figure 2A), which contains only one positive charge. This was easy to do as the core molecule can be simply modified by other functional groups. This would allow us to investigate how modifications could affect organelle-targeting properties. Upon staining the cell, we observed that CDPP-BzBr targeted the mitochondria instead of the ER. The staining properties of CDPP-BzBr were verified by co-staining with Mito-Tracker Deep Red (**Figure 5**). It showed excellent overlap colocalized pattern with Mito-Tracker Deep Red in HeLa cells with a high Pearson's correlation factor of 0.89. This key difference suggests that the zwitterionic property of the functional group is critical for ER staining.

It should be noted that a major component of the phospholipid bilayer of the different membranes of mammalian cells is phosphatidylcholine (PC), a zwitterionic phospholipid. PC has oppositely matching charges to CDPP-$3SO_3$ and CDPP-$4SO_3$, and in theory they would create ideal matching electrostatic interactions. As is clearly seen in the cell staining (Figure 4; Figure S10, Supporting Information), no visible emission from the zwitterionic probes is observed on the different membranes, only selectively targeting the ER. A major function of the ER is glycerophospholipid synthesis, such as PC, via the enzyme CCT located on the ER membrane. The CCT enzyme binds to anionic regions of the ER membrane via electrostatic interactions with its positively charged α-helical M domain (Figure 1). The zwitterionic nature of the probes may find it more favorable to target such locales, as they also have oppositely matching charges. We are currently investigating with more detail the mechanism behind the ER targeting of the probes.

2.4.1. Two-Photon Imaging

The synthesized CDPP derivatives were anticipated to have strong two-photon absorption (2PA) because of their strong electron donating and withdrawing groups.[54] The 2PA measurements of these compounds were carried out using two-photon excited fluorescence (TPEF) technique with a femtosecond pulsed laser source, and comparative TPEF intensity at $f_w = 90\%$ were measured using Rhodamine B as the standard. TPEF intensities were scanned between 820 and 1000 nm at an

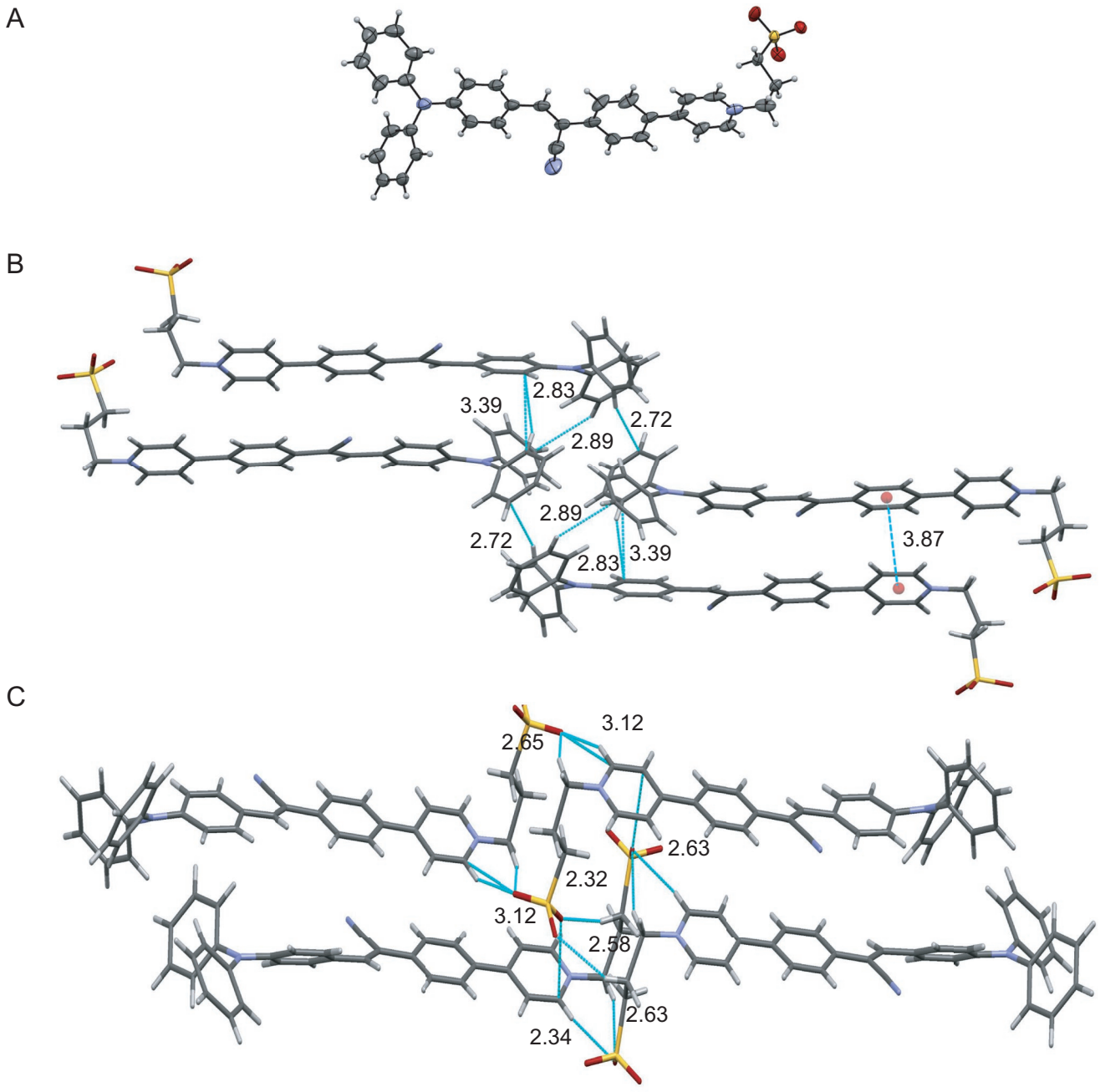

Figure 3. Single crystal structure of CDPP-3SO_3, A) thermal ellipsoid (50%) plot and packing of showing B) CH···π and π···π interactions, and C) CH···O and π···O interactions of CDPP-3SO_3.

interval of 30 nm and respective δ_{2PA} values were calculated. The highest δ_{2PA} value of 162 GM was calculated for CDPP-4SO_3 at 820 nm. The δ_{2PA} values of the two other molecules, CDPP-3SO_3 and CDPP-BzBr, were also calculated and found to be 122 and 71 GM at 820 and 970 nm, respectively (**Figure 6**A). The obtained 2PA values are much higher than most of fluorescence proteins such as EGFP (39 GM).[55] Hence CDPP derivatives may be utilized as good two-photon imaging probes.

The photostability of CDPP-3SO_3, CDPP-4SO_3, CDPP-BzBr, ER-Tracker Red, and Mito-Tracker Red were assessed in parallel, with continuous excitation and sequential scanning with a confocal microscope. The result showed that the emission intensity of CDPP-3SO_3 and CDPP-4SO_3 decreased by about 25% within 80 irradiation scans. In contrast, the fluorescence loss of ER-Tracker Red was around 50% upon irradiation under the same conditions, demonstrating the superior photostability of CDPP-3SO_3 and CDPP-4SO_3 to that of ER-Tracker Red (Figure 6B). CDPP-BzBr showed similar photostability as Mito-Tracker Red (Figure S12, Supporting Information). Moreover, two-photon cell imaging was conducted. As seen

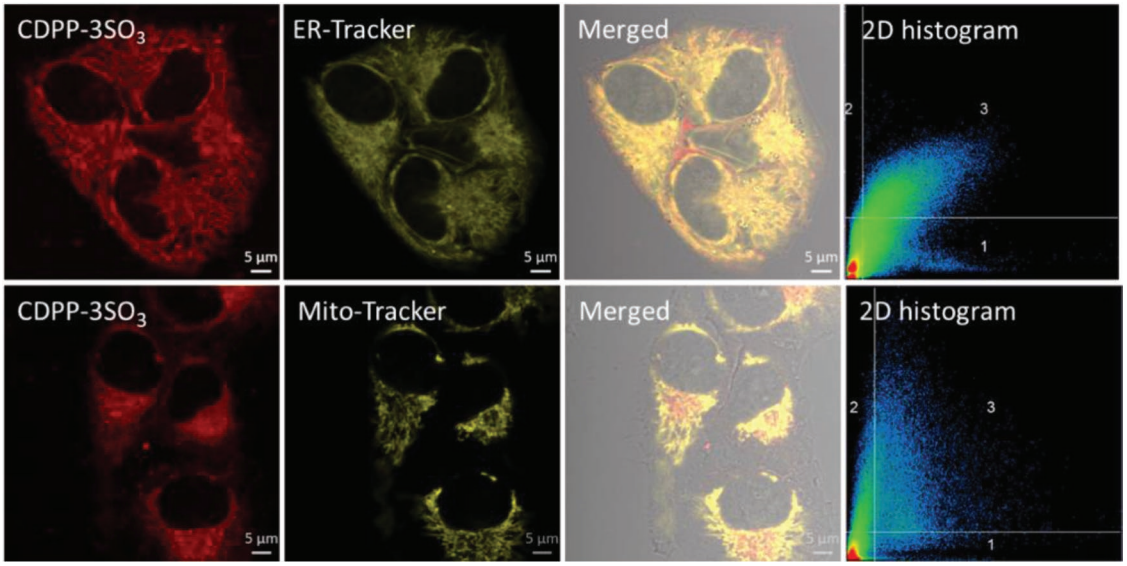

Figure 4. Confocal microscopy imaging of HeLa cells labeled with CDPP-3SO_3 (1×10^{-6} M) and its colocalization with ER-Tracker Red (1×10^{-6} M) ($R = 0.85$) (top) and Mito-Tracker Deep Red (250×10^{-9} M) ($R = 0.55$) (bottom); scale bar = 5 μm.

in Figure 6C,D and Figures S13 and S14 in the Supporting Information, sufficient signals were obtained for CDPP-3SO3, CDPP-4SO3, and CDPP-BzBr under both one-photon and two-photon excitation, indicating all three AIEgens were suitable for two-photon imaging as well as one-photon imaging.

2.4.2. Cytotoxicity and Phototoxicity

The cytotoxicity of CDPP series AIEgens were evaluated by the method of 3-(4,5-dimethyl-2-thiazolyl)-2,5-diphenyltetrazolium bromide (MTT) assay. As shown in Figure S15 in the Supporting Information, CDPP series AIEgens only showed significant toxicity to both COS-7 and HeLa cells when staining concentration was at 40×10^{-6} M. At the working concentration for cell imaging of 1×10^{-6} M, the dyes exhibited minimal toxicity, suggesting that the CDPP AIEgens are suitable for long-term tracking imaging.

Reactive oxygen species (ROS) generation abilities of CDPP derivatives were also investigated by using 9,10-anthracenediyl-bis(methylene)dimalonic acid (ABDA) as the singlet oxygen probe ($^1O_2$) (Figure S16A, Supporting Information). All CDPP derivatives showed good $^1O_2$ generation efficiency at 10×10^{-6} M, CDPP-BzBr showed the best $^1O_2$ generation efficiency with a high consumption rate of ABDA in 2 min (95.86 nmol). Furthermore, the photodynamic therapy (PDT) effect of CDPP-BzBr was investigated. At higher concentrations (10×10^{-6} M or above), it showed excellent anticancer properties, while at lower concentrations (5×10^{-6} M or below), it showed good biocompatibility even under white light irradiation. This demonstrated that CDPP-BzBr can be applied as PDT reagents in higher concentrations (Figure S16B, Supporting Information), as well as long-term tracking fluorescent probes at lower concentrations. In addition, we have also studied IC_{50} values with phototoxicity to HeLa and Cos-7 cells and their IC_{50} values were calculated to be 13.4×10^{-6} and 19.3×10^{-6} M, respectively (Figure S16C,D, Supporting Information).

3. Conclusion

Herein, red emissive fluorescent probes were rationally designed and synthesized. All these probes exhibited AIE activity with emission maximum up to 665 nm. The solid-state efficiency of CDPP-3SO_3 was excellent and found to be 39.3%. Additionally, all these molecules showed excellent

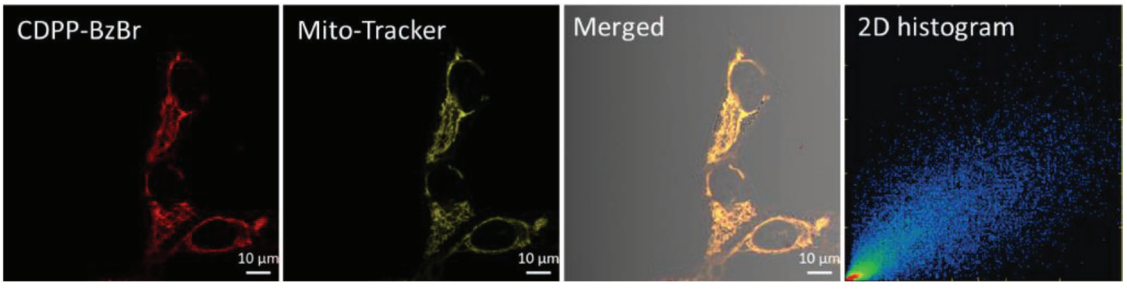

Figure 5. Confocal microscopy imaging of HeLa cells labeled with CDPP-BzBr (10×10^{-6} M) and its colocalization with Mito-Tracker Deep Red (250×10^{-9} M); Pearson's coefficient (R) = 0.89, scale bar = 10 μm.

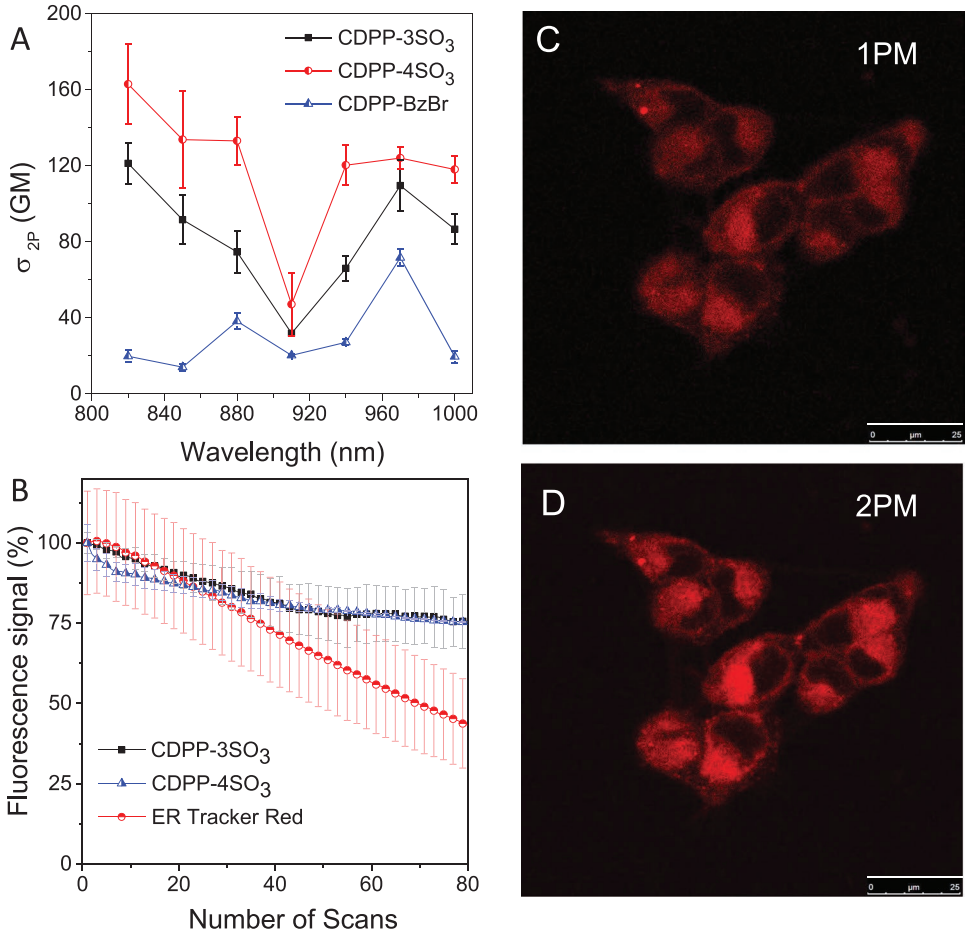

Figure 6. A) Two-photon absorption cross-section of CDPP-3SO_3, CDPP-4SO_3, and CDPP-BzBr; condition: DMSO/water (1:9), concentration: 100×10^{-6} M. B) Signal change in HeLa cells stained with ER-Tracker Red, CDPP-3SO_3, and CDPP-4SO_3 upon continuous scanning by laser light ($\lambda_{ex} = 488$ nm for CDPP-3SO_3 and CDPP-4SO_3; $\lambda_{ex} = 560$ nm for ER-Tracker Red). Confocal images of HeLa cells stained with CDPP-3SO_3 (1×10^{-6} M), $\lambda_{ex} = 480$ nm for C) one-photon microscope (1PM) and 820 nm for D) two-photon microscope (2PM); scale bar = 25 µm.

photostability with some displaying two-photon absorption cross-sections of up to 162 GM. These dyes were found to be good candidates for cell imaging because of high cell biocompatibility, high selectivity, high brightness, low background, and excellent photostability. The zwitterionic AIEgens, CDPP-3SO_3 and CDPP-4SO_3 were successful in imaging the ER in various live cell lines, such as HeLa cells and 143B cells. In contrast, the singly positive charged CDPP-BzBr could only stain the mitochondria. The design strategy demonstrates an easy methodology to develop a variety of different organelle specific efficient red emitters as a platform to study the structure–property relationships regarding such bioimaging probes.

4. Experimental Section

Materials and Instruments: 4-(diphenylamino)benzaldehyde, 2-(4-bromophenyl)acetonitrile, pyridin-4-ylboronic acid, 4-bromo benzyl bromide, 1 3-propane sultone, 1 4-butane sultone, sodium hydroxide, potassium carbonate, and tetrakis(triphenylphosphine)palladium(0) were purchased from Sigma-Aldrich. All the spectroscopic grade solvents such as acetonitrile (ACN), ethanol (EtOH), tetrahydrofuran (THF), dichloromethane (DCM), ethyl acetate (EA), hexane, and DMSO were procured from the Merck Company. All the molecules synthesized were purified by column chromatography and recrystallized using double layer solution diffusion with dichloromethane/hexane or dichloromethane/ethyl acetate and fully characterized by ^{1}H NMR, ^{13}C NMR, and HRMS. ^{1}H and ^{13}C NMR spectra were recorded on a Bruker AV 400 Spectrometer at 400 and 100 MHz in $CDCl_3$ and d_6-DMSO, respectively. Tetramethylsilane (TMS) was used as the internal standard. High-resolution mass spectra were recorded on a GCT premier CAB048 mass spectrometer operating in MALDI-TOF mode. The photoluminescence spectra were measured on a PerkinElmer LS 55 spectrophotometer and Horiba Fluoromax 4 spectrofluorometer. Quantum yields of the solids were recorded on Hamamatsu, C13534 at room temperature with a calibrated integrating sphere system. The lifetime was measured on an Edinburgh FLSP 920 fluorescence spectrophotometer equipped with a Xenon arc lamp (Xe900) and a microsecond flash-lamp (uF900). Single crystal data was collected on a Bruker Smart APEXII CCD diffractometer using graphite monochromated Cu Kα radiation ($\lambda = 1.54178$ Å).

Synthesis of Compound CDPBr: 4-(*N*,*N*-Diphenylamino) benzaldehyde (5.0 g, 18.30 mmol) was dissolved in 100 mL ethanol, 4-bromophenylacetonitrile (4.28 g, 21.96 mmol), and NaOH (0.88 g, 21.96 mmol) were added, and then stirred at room temperature for 3 h. After the reaction completed, the product was purified by recrystallization from EtOH to give the compound CDPBr as a yellow solid. This crude product was purified by silica-gel column chromatography using

DCM/ethyl acetate (v/v = 1:1) as eluent to furnish a yellow solid as product. Yield: 85%.

CDPBr: ^{1}H NMR (400 MHz, $CDCl_3$) ^{1}H NMR (400 MHz, $CDCl_3$) δ 7.76 (d, J = 2.6 Hz, 2H), 7.57–7.48 (m, 4H), 7.40 (s, 1H), 7.37–7.28 (m, 4H), 7.20–7.10 (m, 6H), 7.05 (d, J = 5.2 Hz, 2H). ^{13}C NMR (101 MHz, $CDCl_3$) ^{13}C NMR (101 MHz, $CDCl_3$) δ 149.58, 145.86, 141.39, 133.43, 131.48, 130.16, 128.99, 126.53, 125.37, 125.19, 123.92, 121.97, 120.04, 117.81, 105.72., HRMS, *m/z*: ($[M]^+$), calculated: 450.0732, found: 450.0714.

Synthesis of Compound CDPP: Compound CDPBr (1.0 g, 2.22 mmol), (4-hydroxylphenyl)boronic acid (0.33 mg, 2.66 mmol), potassium carbonate (3.07 g, 22.21 mmol), and $Pd(PPh_3)_4$ (25.41 mg, 0.01 mmol) were added in 60 mL THF and 9 mL water into a 250 mL two-necked round bottom flask which was equipped with a condenser under nitrogen. The mixture was heated to reflux overnight with stirring. After cooling to room temperature, the mixture was extracted with DCM for three times. The organic phase was collected, washed with water, and then dried over anhydrous sodium sulfate. After solvent evaporation, the crude product was purified by silica-gel column chromatography using DCM/ethyl acetate (v/v = 2:3) as eluent to furnish an orange solid as product. Yield: 75%.

CDPP: ^{1}H NMR (400 MHz, $CDCl_3$) δ 8.67 (d, J = 5.3 Hz, 2H), 7.79 (dd, J = 15.4, 8.7 Hz, 2H), 7.70 (d, J = 8.5 Hz, 1H), 7.65 (d, J = 8.4 Hz, 1H), 7.57 (m, 4H), 7.36–7.24 (m, 5H), 7.21–7.01 (m, 8H), 6.82 (d, J = 8.8 Hz, 1H). ^{13}C NMR (101 MHz, $CDCl_3$) δ 149.76, 149.61, 149.11, 146.57, 145.85, 145.80, 143.70, 141.54, 137.98, 137.40, 135.20, 133.72, 130.66, 130.25, 129.07, 128.99, 128.93, 127.05, 126.90, 125.69, 125.45, 125.19, 125.16, 125.00, 123.93, 123.85, 120.86, 120.76, 120.13, 120.03, 119.59, 117.96, 108.89, 105.96. HRMS, *m/z*: ($[M]^+$), calculated: 449.1892, found: 449.1884.

General Synthesis of CDPP Sulfonate: To an oven dried round bottom flask sealed with rubber stopper, CDPP (1.6 mmol) and sultones (1,3 propane sultone/1,4 butane sultone, 1.6 mmol) were added, followed by the addition of dry acetonitrile (10 mL). The reaction mixture was refluxed at 95 °C for 6–8 h. Then, the mixture evaporated under reduced pressure to afford the crude product which was further purified by column chromatography using MeOH/DCM mixture as an eluent to furnish a red solid as product. Yield: 75–80%.

CDPP-3SO$_3$: ^{1}H NMR (400 MHz, DMSO) δ 9.11 (d, J = 6.8 Hz, 2H), 8.56 (d, J = 6.8 Hz, 2H), 8.21 (d, J = 8.6 Hz, 2H), 8.13 (s, 1H), 7.96 (d, J = 8.6 Hz, 2H), 7.91 (d, J = 8.9 Hz, 3H), 7.41 (t, J = 7.8 Hz, 3H), 7.19 (dd, J = 16.2, 7.6 Hz, 5H), 6.96 (d, J = 8.8 Hz, 2H), 4.72 (t, J = 6.8 Hz, 2H), 2.45 (t, J = 8.2 Hz, 2H), 2.29–2.23 (m, 2H). ^{13}C NMR (101 MHz, CDCl3) δ 154.76, 150.14, 145.61, 143.93, 143.28, 138.52, 132.34, 130.59, 128.94, 127.79, 126.05, 125.30, 124.78, 124.23, 124.04, 119.53, 117.51, 104.48, 59.84, 29.46, 20.73. HRMS, *m/z*: ($[M+H]^+$), calculated: 572.2008, found: 572.2015.

CDPP-4SO$_3$: ^{1}H NMR (400 MHz, DMSO) δ 9.12 (d, J = 6.9 Hz, 2H), 8.58 (d, J = 6.9 Hz, 2H), 8.22 (d, J = 8.7 Hz, 2H), 8.14 (s, 1H), 7.94 (dd, J = 18.7, 8.8 Hz, 3H), 7.41 (t, J = 7.9 Hz, 3H), 7.25–7.12 (m, 5H), 6.96 (d, J = 8.9 Hz, 2H), 4.61 (t, J = 7.2 Hz, 2H), 2.51–2.41 (m, 2H), 2.05 (dd, J = 14.6, 7.6 Hz, 2H), 1.60 (dt, J = 15.3, 7.6 Hz, 2H). ^{13}C NMR (101 MHz, $CDCl_3$) δ 154.76, 150.11, 145.47, 143.99, 143.31, 138.44, 132.26, 130.55, 128.90, 127.81, 125.99, 125.26, 124.67, 124.11, 124.02, 119.38, 117.58, 104.14, 58.45, 46.02, 26.21, 17.67. HRMS, *m/z*: ($[M+H]^+$), calculated: 586.2164, found: 586.2190.

Synthesis of CDPP-BzBr: Into a 50 mL two-necked round bottom flask equipped with a condenser was dissolved CDPP (1000 mg, 2.22 mmol) in 200 mL acetonitrile. 4-bromo benzyl bromide (662 mg, 2.67 mmol) was then added and the mixture was heated to reflux for 8 h. After cooling to room temperature, the mixture was poured into diethyl ether. The dark red precipitates formed were filtered by suction filtration. Further, the crude product which was further purified by column chromatography using MeOH/DCM mixture as an eluent to furnish a red solid as product. Yield: 80%.

CDPP-BzBr: ^{1}H NMR (400 MHz, $CDCl_3$) δ 9.13 (d, J = 5.3 Hz, 2H), 8.21 (d, J = 5.7 Hz, 2H), 7.83 (d, J = 8.3 Hz, 2H), 7.73 (dd, J = 8.4, 4.2 Hz, 4H), 7.52 (s, 1H), 7.45 (s, 4H), 7.24 (dd, J = 14.6, 6.7 Hz, 4H), 7.07 (d, J = 7.0 Hz, 6H), 6.93 (d, J = 8.8 Hz, 2H), 5.84 (s, 2H). ^{13}C NMR (101 MHz, $CDCl_3$) δ 154.77, 150.13, 145.47, 143.88, 143.34, 138.57, 132.10, 131.91, 131.22, 130.65, 130.37, 128.96, 127.90, 126.00, 125.31, 124.68, 124.17, 124.10, 123.75, 119.37, 117.61, 104.07, 62.12. HRMS, *m/z*: ($[M]^+$), calculated: 618.1539, found: 618.1553.

Two-Photon Absorption Cross-Sections Measurement: A two-photon excitation fluorescence cross-section was measured by two-photon excitation fluorescence method using rhodamine B as a reference. The excitation source for two-photon excitation was a femtosecond optical parametric amplifier (Coherent OPerA Solo) pumped by an amplified Ti:sapphire system (Coherent Legend Elite system) and then detected with a spectrometer (Acton SpectraPro-500i) coupled to a CCD. The TPA cross-section (δ) of the sample was calculated at each wavelength according to the following formula[56]

$$\delta = \delta_{\text{ref}} \frac{\phi_{\text{ref}}}{\phi} \frac{c_{\text{ref}}}{c} \frac{\eta_{\text{ref}}}{\eta} \frac{F}{F_{\text{ref}}} \quad (1)$$

where δ is the cross-sectional value, c is the concentration of the solution, n is the refractive index of the solution, F is the two-photon excited fluorescence integral intensity of the light emitted at the excitation wavelength, and ϕ is the fluorescence quantum yield.

Cell Imaging and Confocal Colocalization: HeLa cells and 143B cells were cultured in the Dulbecco's Modified Eagle Medium (DMEM) containing 10% fetal bovine serum (FBS) and antibiotics (100 units mL^{-1} penicillin and 100 mg mL^{-1} streptomycin) in a 5% CO_2 humidity incubator at 37 °C. After cells were incubated with CDPP derivatives and the commercial probes at 37 °C for 30 min, the medium was removed and the cells were rinsed with phosphate buffer saline (PBS) three times and then imaged under a confocal microscope (ZEISS, LSM710). The excitation was 488 nm for CDPP derivatives, 560 nm for ER-Tracker Red, and 633 nm for Mito-Tracker Deep Red.

Cytotoxicity Study in the Dark and under Light Irradiation: Cells were seeded in 96-well plates (Costar, IL, U.S.A.) at a density of 5000 cells per well. After overnight culturing, the medium in each well was replaced by 100 µL of fresh medium containing different concentrations of AIEgens. After 24 h incubation, 10 µL of MTT solution (5 mg mL^{-1} in PBS) was added into each well and incubated for 4 h. After a further 30 min of incubation under light irradiation, in which another array of plates in the dark was used as the control, 100 µL of DMSO was added to each well and then vibrated for 15 min. The absorption of each well at 595 nm was recorded via a plate reader (PerkinElmer Victor3TM). Each trial was performed with 6 wells parallel.

Photostability: The cells were imaged using a confocal microscope (Zeiss Laser Scanning Confocal Microscope; LSM7 DUO) and analyzed using ZEN 2009 software (Carl Zeiss). The concentrations of all the three probes were 1×10^{-6} M. CDPP-3SO$_3$ and CDPP-4SO$_3$ were excited at 488 nm for one-photon imaging (2% laser power). ER-Tracker Red was excited at 560 nm for one-photon imaging (2% laser power). The scanning speed was 0.93 s per scan, and the repeated image scans were taken 80 times. The first scan of CDPP-3SO$_3$, CDPP-4SO$_3$, and ER-Tracker Red was set to 100%, followed by which the pixel intensity values were averaged and plotted against the scan number. The resulting curve represents the bleaching rate.

[CCDC 1963718 contains the supplementary crystallographic data for this paper. These data can be obtained free of charge from The Cambridge Crystallographic Data Centre via www.ccdc.cam.ac.uk/data_request/cif.]

Supporting Information

Supporting Information is available from the Wiley Online Library or from the author.

Acknowledgements

P.A. and W.H. contributed equally to this work. This work was partially supported by the National Natural Science Foundation of China

(Grant No. 21788102), the Research Grants Council of Hong Kong (16308016, 16308116, C6009-17G, and AoE/P-02/12), the Innovation and Technology Commission (ITC-CNERC14SC01 and ITCPD/17-9), and the Science and Technology Plan of Shenzhen (JCYJ20180507183832744 and JCYJ20160229205601482).

Conflict of Interest

The authors declare no conflict of interest.

Keywords

aggregation-induced emission, bioimaging, endoplasmic reticulum, zwitterionic

Received: November 6, 2019
Revised: December 12, 2019
Published online:

[1] J. D. Marth, *Nat. Cell Biol.* **2008**, *10*, 1015.
[2] K. Mesa, *Yale J. Biol. Med.* **2015**, *88*, 100.
[3] R. A. Weinberg, *Sci. Am.* **1996**, *275*, 62.
[4] C. P. Satori, M. M. Henderson, E. A. Krautkramer, V. Kostal, M. D. Distefano, E. A. Arriaga, *Chem. Rev.* **2013**, *113*, 5699.
[5] K. W. Osteryoung, J. Nunnari, *Science* **2003**, *302*, 1698.
[6] A. H. Futerman, G. van Meer, *Nat. Rev. Mol. Cell Biol.* **2004**, *5*, 554.
[7] B. Alberts, D. Bray, K. Hopkin, A. Johnson, J. Lewis, M. C. Raff, K. Roberts, P. Walter, *Essential Cell Biology*, Garland Science, New York **2014**.
[8] H. F. Steedman, *Q. J. Microsc. Sci.* **1950**, *91*, 477.
[9] A. S. Klymchenko, *Acc. Chem. Res.* **2017**, *50*, 366.
[10] H. Zhu, J. Fan, J. Du, X. Peng, *Acc. Chem. Res.* **2016**, *49*, 2115.
[11] C.-J. Zhang, Q. Hu, G. Feng, R. Zhang, Y. Yuan, X. Lu, B. Liu, *Chem. Sci.* **2015**, *6*, 4580.
[12] F. Xue, P. Wei, X. Ge, Y. Zhong, C. Cao, D. Yu, T. Yi, *Dyes Pigm.* **2018**, *156*, 285.
[13] C. Gao, Y. Tian, R. Zhang, J. Jing, X. Zhang, *Anal. Chem.* **2017**, *89*, 12945.
[14] Y. Li, Y. Wu, J. Chang, M. Chen, R. Liu, F. Li, *Chem. Commun.* **2013**, *49*, 11335.
[15] M. H. Teiten, L. Bezdetnaya, P. Morlière, R. Santus, F. Guillemin, *Br. J. Cancer* **2003**, *88*, 146.
[16] F. Hu, B. Liu, *Org. Biomol. Chem.* **2016**, *14*, 9931.
[17] S. J. Sahl, S. W. Hell, S. Jakobs, *Nat. Rev. Mol. Cell Biol.* **2017**, *18*, 685.
[18] G. Vicidomini, P. Bianchini, A. Diaspro, *Nat. Methods* **2018**, *15*, 173.
[19] L. Schermelleh, A. Ferrand, T. Huser, C. Eggeling, M. Sauer, O. Biehlmaier, G. P. C. Drummen, *Nat. Cell Biol.* **2019**, *21*, 72.
[20] P. Alam, N. L. C. Leung, Y. Cheng, H. Zhang, J. Liu, W. Wu, R. T. K. Kwok, J. W. Y. Lam, H. H. Y. Sung, I. D. Williams, B. Z. Tang, *Angew. Chem.* **2019**, *131*, 4584.
[21] H. Nie, K. Hu, Y. Cai, Q. Peng, Z. Zhao, R. Hu, J. Chen, S.-J. Su, A. Qin, B. Z. Tang, *Mater. Chem. Front.* **2017**, *1*, 1125.
[22] Z. He, C. Ke, B. Z. Tang, *ACS Omega* **2018**, *3*, 3267.
[23] Z. Zhao, B. He, B. Z. Tang, *Chem. Sci.* **2015**, *6*, 5347.
[24] Y. Hong, J. W. Y. Lam, B. Z. Tang, *Chem. Soc. Rev.* **2011**, *40*, 5361.
[25] H. Wang, E. Zhao, J. W. Y. Lam, B. Z. Tang, *Mater. Today* **2015**, *18*, 365.
[26] J. Qian, B. Z. Tang, *Chem* **2017**, *3*, 56.
[27] Q. Wan, Q. Huang, M. Liu, D. Xu, H. Huang, X. Zhang, Y. Wei, *Appl. Mater. Today* **2017**, *9*, 145.
[28] F. Hu, S. Xu, B. Liu, *Adv. Mater.* **2018**, *30*, 1801350.
[29] S. Wang, F. Hu, Y. Pan, L. G. Ng, B. Liu, *Adv. Funct. Mater.* **2019**, *29*, 1902717.
[30] P. Alam, N. L. C. Leung, H. Su, Z. Qiu, R. T. K. Kwok, J. W. Y. Lam, B. Z. Tang, *Chem. - Eur. J.* **2017**, *23*, 14911.
[31] Y. Tatenaka, H. Kato, M. Ishiyama, K. Sasamoto, M. Shiga, H. Nishitoh, Y. Ueno, *Biochemistry* **2019**, *58*, 499.
[32] H. Shi, J. Liu, J. Geng, B. Z. Tang, B. Liu, *J. Am. Chem. Soc.* **2012**, *134*, 9569.
[33] C. Zhang, S. Jin, K. Yang, X. Xue, Z. Li, Y. Jiang, W.-Q. Chen, L. Dai, G. Zou, X.-J. Liang, *ACS Appl. Mater. Interfaces* **2014**, *6*, 8971.
[34] J. M. Meinig, L. Fu, B. R. Peterson, *Angew. Chem., Int. Ed.* **2015**, *54*, 9696.
[35] S. Zheng, C. Huang, X. Zhao, Y. Zhang, S. Liu, Q. Zhu, *Spectrochim. Acta, Part A* **2018**, *189*, 231.
[36] L. Shi, X. Gao, W. Yuan, L. Xu, H. Deng, C. Wu, J. Yang, X. Jin, C. Zhang, X. Zhu, *Small* **2018**, *14*, 1800223.
[37] C.-J. Zhang, X. Cai, S. Xu, R. Zhan, W. Jien, B. Liu, *Chem. Commun.* **2017**, *53*, 10792.
[38] S. Hussain, W. Du, M. Zhang, B. Fang, G. Zhang, R. Su, K. Nan, Q. Zhang, X. Tian, Y. Tian, Y. Chen, *J. Mater. Chem. B* **2018**, *6*, 1943.
[39] B. Dong, Y. Lu, N. Zhang, W. Song, W. Lin, *Anal. Chem.* **2019**, *91*, 5513.
[40] W. Song, B. Dong, Y. Lu, X. Kong, A. H. Mehmood, W. Lin, *Anal. Methods* **2019**, *11*, 4450.
[41] M. Wang, R. J. Kaufman, *Nat. Rev. Cancer* **2014**, *14*, 581.
[42] D. Naon, M. Zaninello, M. Giacomello, T. Varanita, F. Grespi, S. Lakshminaranayan, A. Serafini, M. Semenzato, S. Herkenne, M. I. Hernández-Alvarez, A. Zorzano, D. De Stefani, G. W. Dorn, L. Scorrano, *Proc. Natl. Acad. Sci. USA* **2016**, *113*, 11249.
[43] W. Lin, B. Popko, *Nat. Neurosci.* **2009**, *12*, 379.
[44] P. Strzyz, *Nat. Rev. Mol. Cell Biol.* **2019**, *20*, 453.
[45] W. Li, J. Yang, L. Luo, M. Jiang, B. Qin, H. Yin, C. Zhu, X. Yuan, J. Zhang, Z. Luo, Y. Du, Q. Li, Y. Lou, Y. Qiu, J. You, *Nat. Commun.* **2019**, *10*, 3349.
[46] F. Gibellini, T. K. Smith, *IUBMB Life* **2010**, *62*, spc1.
[47] R. B. Cornell, I. C. Northwood, *Trends Biochem. Sci.* **2000**, *25*, 441.
[48] P. Fagone, S. Jackowski, *Biochim. Biophys. Acta, Mol. Cell Biol. Lipids* **2013**, *1831*, 523.
[49] R. B. Cornell, *Biochim. Biophys. Acta, Mol. Cell Biol. Lipids* **2016**, *1861*, 847.
[50] S. G. Taneva, J. M. C. Lee, R. B. Cornell, *Biochim. Biophys. Acta, Biomembr.* **2012**, *1818*, 1173.
[51] C. Y. Y. Yu, H. Xu, S. Ji, R. T. K. Kwok, J. W. Y. Lam, X. Li, S. Krishnan, D. Ding, B. Z. Tang, *Adv. Mater.* **2017**, *29*, 1606167.
[52] C. DeBruler, B. Hu, J. Moss, J. Luo, T. L. Liu, *ACS Energy Lett.* **2018**, *3*, 663.
[53] A. Hassner, D. Birnbaum, L. M. Loew, *J. Org. Chem.* **1984**, *49*, 2546.
[54] Z. Zheng, T. Zhang, H. Liu, Y. Chen, R. T. K. Kwok, C. Ma, P. Zhang, H. H. Y. Sung, I. D. Williams, J. W. Y. Lam, K. S. Wong, B. Z. Tang, *ACS Nano* **2018**, *12*, 8145.
[55] M. Drobizhev, N. S. Makarov, S. E. Tillo, T. E. Hughes, A. Rebane, *Nat. Methods* **2011**, *8*, 393.
[56] Q. Zhang, X. Tian, H. Zhou, J. Wu, Y. Tian, *Materials* **2017**, 10, 223.

